Evaluation and Projections of Summer Daily Precipitation over Northeastern China in an Optimal CMIP6 Multi-model Ensemble

LI Zi-Liang

liziliang@ouc.edu.cn

Ocean University of China https://orcid.org/0000-0003-3179-685X

Jiao Xin-Zhe

Ocean University of China - Laoshan Campus: Ocean University of China

Research Article

Keywords: CMIP6, Evaluation and Projection, HMME, Precipitation

Posted Date: November 25th, 2023

DOI: https://doi.org/10.21203/rs.3.rs-3505005/v1

Version of Record: A version of this preprint was published at Climate Dynamics on April 10th, 2024. See the published version at https://doi.org/10.1007/s00382-024-07201-6.

Abstract

In the early summer of 2022, the average precipitation in Northeastern China (NEC) was 144.9 mm, which was 62% higher than the normal precipitation (89.5 mm), and was the largest amount of precipitation since historical records began in 1951. Based on the CN05.1 precipitation data, the summer precipitation simulated by the sixth Coupled Model Intercomparison Project (CMIP6) model was evaluated in the NEC region. The model performs well in reproducing the climatological spatial distribution and interannual variability of precipitation. The simulation effect of a multi-model ensemble is better than that of a single model. The top three optimal models (EC-Earth3-Veg, EC-Earth3 and MPI-ESM1-2-LR) can constitute the optimal model ensemble (HMME). Compared with a single model and an ensemble of all 20 models, HMME significantly reduces the wet bias on the southeastern side of the Da Xing-AN Ling Mountains. HMME projects that daily precipitation will show an increasing trend in NEC region from 2015 to 2100. Under the two scenarios of SSP245 and SSP585, the increase rates of precipitation are 0.05mm/10a and 0.15mm/10a respectively. Although precipitation trends varied between scenarios at different times of the year, by the end of the 21st century, precipitation increased significantly across the region, with the largest increase in precipitation located in the southern part of northeastern China.

1. Introduction

The Sixth Assessment Report of the Intergovernmental Panel on Climate Change (IPCC) stated that global temperatures have risen by 1.1°C from 1850–1900 to 2010–2019, implying a high sensitivity of the climate system (IPCC, 2023). In particular, changes in precipitation exhibit substantial uncertainty. Although temperature is a key driver of precipitation anomalies, precipitation is not always associated with temperature changes because of the dynamical environment (Xu et al., 2023). Therefore, it is essential to project the future changes of precipitation.

Northeastern China (NEC) produces nearly a quarter of China's total grain. Summer precipitation, which accounts for more than 65% of the total annual precipitation in this region (Liang et al., 2011), provides water security for crops during the critical period of water. Therefore, the spatial-temporal variation of summer precipitation plays a key role in agricultural production and water mobilization in NEC. Previous studies show that the causes of summer precipitation anomalies over NEC are varied. The East Asian summer monsoon and other mid-high latitude climate systems are the main factors influencing the climate changes in NEC (Yao and Dong, 2000; Shen et al., 2011; Gao et al., 2014a; Sun et al., 2017; Gao and Gao, 2018; Han et al., 2018; Zhao et al., 2018). Meanwhile, changes of external forcings like sea surface temperature anomaly or sea ice variability drive precipitation anomalies (e.g., Wu et al., 2011; Gao et al., 2014b; Han et al., 2018; Han et al., 2021). In terms of complex climate system, summer precipitation over NEC varies with region (Liu et al., 2010; Mao et al., 2022) and its spatial-temporal variation is unable to be simulated and projected very well.

Climate model is one of the most important tools for climate simulation and projection. The Coupled Model Intercomparison Project (CMIP) collected a large amount of data produced by different global

climate models (GCMs). In recent years, the 6th Phase of CMIP (CMIP6) has been generated from models with higher spatial resolution and more complex physical processes compared to the previous phase (Eyring et al., 2016; Stouffer et al., 2017; Zhou et al., 2019). A new database of the Shared Economic Pathways (SSP) was developed to integrate climate change and economic development in the CMIP6 scenarios (Eyring et al., 2016; Stouffer et al., 2017; Zhou et al., 2019). Up to now, several studies have demonstrated that CMIP6 models generally exhibit satisfactory simulation performance in modelling annual mean and seasonal precipitation on the global scale (e.g., Du et al., 2022; Donat et al., 2023). However, due to the different settings in climate model, such as physical processes, initial conditions, and parameterization schemes, the simulation performance of each model varies from region to region. Dong and Dong (2021) studied the performance of the CMIP6 models to reproduce the spatial distribution and trends of extreme precipitation over East Asia. There was generally a wet bias in western China and a dry bias in South Asian. He et al. (2023) obtained a similar result that CMIP6 models underestimated South Asian summer rainfall. On the regional climate change over China, Xin et al. (2020) evaluated eight models, most of which underestimated the gradient of precipitation decrease from southeast to northwest. Especially for the “southern flood and northern drought” rainfall pattern in China, only two models were able to partially reproduce it. It is notable that the uncertainty in climate projections arises from the model uncertainty, scenario uncertainty and internal variability. By using analysis of variance, Jia et al. (2023) indicated that the model uncertainty was the dominant factor in projection. Thus, it might be of primary importance for the credibility of future projection to evaluate the performance of CMIP6 models on the regional scale.

Several metrics have long been used to measure the simulation performance of climate models, such as correlation coefficient (CC), root-mean-square error (RMSE), standard deviation (STD), Taylor Skill Score (TS) and the interannual variability skill score (IVS) (Taylor, 2001; Chen et al., 2011). In general, more than one indicator is considered in order to evaluate the performance of model. Many studies indicated that models have different simulation performances in different sub-regions (Jiang et al., 2020; Dong and Dong, 2021). To cope with the model uncertainty from single model, the multi-model ensemble has been used to simulate and project (Xin et al., 2020; Zhu et al., 2020).

Additionally, the simulation performance of the multi-model ensemble is also related to the number of members (Pierce et al., 2009). Therefore, based on the evaluation of simulations, more appropriate models could be considered while averaging the projection of a variable. Unfortunately, the optimal model ensemble with high scores (HMME) selected by evaluation of a large region does not apply to all sub-regions. For example, the HMME selected by the performance in simulating temperature and precipitation in China did not show better performance than the all-model ensemble (AMME) in summer precipitation over sub-region (Yang et al., 2021). However, there has been limited works devoted to evaluating the ensemble behaviors of CMIP6 models in sub-region, particularly in simulating precipitation.

Tao et al. (2016) evaluated the simulation ability of the CMIP5 models for temperature across three provinces in NEC. They identified four models that exhibited superior predictive performance. However, whether the models of the CMIP6 models perform well in simulating summer precipitation is still needed

to evaluate. This study aims to explore the model performance in simulating the spatial-temporal distribution summer precipitation over NEC and get the future projection of possible precipitation changes. The remainder of this study is structured as follows: Section 2 describes our data and methods. Focused on the better use of available models, the long-term precipitation simulated by the historical experiment were compared with observation in section 3. And possible future changes of precipitations during 2015–2100 under the scenarios SSP245 and SSP585 were also analyzed in section 4. And section 5 provides a summary of our findings.

2. Data and methods

2.1 Data

The NEC region for this study ranges from 38°N-55°N and 118°E-136°E. The observed daily precipitation amounts were selected from the CN05.1 data set provided by the China National Climate Center, which are interpolated from station observations using the Angular distance weighting (ADW) interpolation method at a horizontal resolution of 0.25°×0.25° (Xu et al., 2009; Wu and Gao, 2013).

This study evaluated the historical summer precipitation (1979–2014) simulated by 20 CMIP6 models, from which the top three optimally ranked models (EC-Earth3-Veg EC-Earth3 MPI-ESM1-2-LR) were selected for future climate projections (2015–2100) under the SSP245 and SSP585 scenarios. The model-name, institute information, time Correlation coefficient, resolution of the GCMs used in this study are listed in Table 1. Due to the different resolutions of the models, the observed and modeled precipitation data were uniformly interpolated onto a grid with resolution of 0.5°×0.5° using bilinear interpolation. The historical period selected for this paper is 1979–2014, the future projection period is 2015–2100, and the climate base period is selected as 1981–2010.

2.2 Methods

To evaluate CMIP6 model performance for precipitations with respect to spatial distribution and interannual variation, we used three evaluation methods in this study: the Taylor skill score (TSS; Taylor, 2001), the interannual variability skill score (IVS; Chen et al., 2011), and the Comprehensive Rating Index (CRI; Jiang et al., 2015).

The Taylor Skill Score (TS; Taylor, 2001) was used to rank GCM in capturing the spatial pattern of precipitation. Taylor diagrams provide spatial correlation coefficients (SCC), centered RMSEs, and standard deviation ratios (SDR) as measures of consistency in the spatial distributions of the model and observations. The TS was calculated as follows:

$$\mathrm{TS} = \frac{(1+\mathrm{SCC})^2}{(\mathrm{SDR}+\frac{1}{\mathrm{SDR}})^2}$$

1

where SDR is the ratio of standard deviation and SCC is the spatial correlation coefficient between modeled and observation data. TS varies from 0 to 1, and a larger TS indicates relatively better performance of a model.

The performance of a model in simulating the interannual variability was estimated using the skill score IVS (Chen et al., 2011; Jiang et al., 2015), which was used to verify that the models can simulate the interannual variability in the observations well and was calculated as follows:

$$IVS = (\frac{STD_m}{STD_o} - \frac{STD_o}{STD_m})^2$$

2

where STD_m and STD_o are the standard deviation of modeled and observed data, respectively. The IVS for each grid point were first calculated, and the mean IVS for the NEC region was then calculated. IVS is a symmetric variability statistic that can filter the interdecadal signal and measure the similarity between the simulated and observed inter-annual variability. The IVS closer to zero indicate that the CMIP6 model can simulate similarly to the observations.

Models are effectively ranked using the Comprehensive Rating Index (CRI) (Jiang et al., 2015). The formula of CRI is given as follows:

$$CRI = 1 - \frac{1}{n \times m} \sum_{i=1}^{m} rank_i$$

3

where m is the number of models and n is the number of metrics. The rankings used in this paper to calculate the CRI are based on RESM, SDR, SCC, and IVS, and models that are more consistent with observations are ranked higher. Thus, the closer the CRI value is to 1, the higher the model simulation skill.

Table 1
General Information on selected GCMs from the CMIP6 used in this study

No.	Model Name	Resolution (Lat × Lon)	Country	Agency	Time Correlation Coefficient
1	ACCESS-CM2	192×144	Australia	CSIRO-ARCCSS	0.23
2	ACCESS-ESM1-5	192×145	Australia	CSIRO	0.18
3	BCC-CSM2-MR	320×160	China	BCC	0.03
4	CanESM5	128×64	Canada	CCC-ma	0.12
5	CESM2	288×192	USA	NCAR	-0.05
6	CESM2-WACCM	288×192	USA	NCAR	0.16
7	EC-Earth3	512×256	Europe	EC-Earth	-0.07
8	EC-Earth3-Veg	512×256	Europe	EC-Earth	-0.09
9	FGOALS-g3	180×80	China	CAS	-0.15
10	GFDL-CM4	280×180	USA	NOAA GFDL	0.40*
11	GFDL-ESM4	280×180	USA	NOAA GFDL	-0.16
12	INM-CM4-8	180×120	Russia	INM	0.10
13	INM-CM5-0	180×120	Russia	INM	-0.25
14	IPSL-CM6A-LR	144×143,	France	IPSL	0.07
15	MIROC6	256×128	Japan	AORI	0.06
16	MPI-ESM1-2-HR	384×192	Germany	MPI-M	-0.19
17	MPI-ESM1-2-LR	192×96	Germany	MPI-M	-0.16
18	MRI-ESM2-0	320×160	Japan	MRI	0.06
19	NorESM2-LM	144×96	Norway	NCC	-0.15
20	NorESM2-MM	288×192	Norway	NCC	0.10

Note: * indicates passing the 95% significance test.

3. Historical period simulation assessment

The performance of different CMIP6 models in simulating summer precipitation from 1979 to 2014 was firstly evaluated. Figure 1 shows the historical simulated (20 CMIP6 models) and observed regional mean summer daily precipitation and its standard deviation in NEC during 1979–2014. The mean summer daily precipitation in NEC region was 3.70 mm/day, and 14 out of 20 models overestimated the summer

precipitation, and 4 of them, CESM2, CESM2-WACCM, INM-CM4-8, and INM-CM5-0, had a relative deviation of more than 40% from the observations. The GFDL-ESM4 simulations were closest to observations, underestimating by only 0.02 mm/day. With the exception of CESM2 and CESM2-WACCM, the standard deviation of most of the models and observations (0.58 mm/day) are in general agreement, indicating that the models can reproduce the intensity of interannual variability of precipitation.

To further analyze the bias of the spatial distribution by different CMIP6 modeled precipitation, the spatial distribution of mean daily precipitation and its deviation in the NEC region simulated by CMIP6 models are given in Figure.2. It can be noted that there is considerable spatial heterogeneity in the bias of different individual models. The observation results (Figure.2b) show that summer precipitation in the NEC region as a whole is characterized by a spatial distribution with more in the southeast and less in the west of the region, and its average daily precipitation ranges from 1.96 to 7.06 mm/day with a large spatial variation. The high precipitation centers in the southern part of NEC and the east side of the Da Xing-AN Ling may be related to the dominance of the summer wind water vapor transport in East Asia (Sun et al., 2017), as well as the better water vapor conditions along the Southeast coast and the topographic blocking effect of the Da Xing-AN Ling (He et al., 2020).

The spatial correlation coefficients (SCC) between the modeled data and observations range from 0.37 to 0.92 (passing the 95% significance test), indicating that the CMIP6 model can basically reproduce the spatial distribution characteristics of precipitation. The spatial distribution of precipitation simulated by EC-Earth3, EC-Earth3-Veg, MPI-ESM-1-2-LR, and MPI-ESM-1-2-HR is closest to that of observations, with the R greater than 0.80. Corresponding to the larger dry bias in regional mean modeled precipitation, ACCESS-CM2, BCC-CSM2-MR, and FGOALS-g3 underestimated precipitation over much of the NEC region. The remaining models with large bias from observed precipitation overestimate precipitation across the region, with positive deviations concentrated on the southeastern side of the Da Xing-AN Ling, where the relative bias exceeds 90%. There is a significant difference in the centers of high precipitation simulated by the CMIP6 model. Most of the models can reasonably simulate the precipitation center on the east side of the Da Xing-AN Ling, and the model simulation bias are small. On the other hand, the modeled precipitations in the southern part of NEC exhibit large uncertainties (Figure.2a), and there is a north-south bias in the location of the precipitation center. Among them, the locations of precipitation centers simulated by CanESM5 and FGOALS-g3 models are significantly northward.

Taylor diagrams can provide a way of graphically summarizing how closely a set of modeled patterns matches observations. These diagrams are especially useful in gauging the relative skill of many different models (Fig. 3). More than half of the model spatial distributions have smaller standard deviations than observations, suggesting that the modeled precipitation is smoother relative to observations. The INM-CM5-0 model generally overestimates precipitation, with greater relative bias in the center of precipitation low. GFDL-ESM4, although the best simulation of regional average precipitation, underestimates precipitation in major precipitation centers and overestimates precipitation in arid regions in the west, resulting in a poor reproduction of the decreasing precipitation gradient from southeast to northwest. However, model INM-CM5-0 and GFDL-ESM4 simulate less variability in the spatial gradient of

precipitation. In terms of the centered RMSE, most of the models have RMSE less than 1, and the models EC-Earth3, EC-Earth3-Veg and MPI-ESM1-2-LR simulate precipitation with less difference from observation. Overall, the EC-Earth3 model is optimal for modeling the spatial distribution of precipitation in the climate state.

In addition to spatial variability, summer precipitation in NEC exhibits more pronounced interannual and interdecadal variability (Liang et al., 2011). A single model or an ensemble of multiple models has a poor ability to simulate precipitation time series. The simulation accuracy of precipitation is relatively low in both climate and weather models. The simulation ability of the CMIP5 model for precipitation in China is much less easy than that of temperature, and it is found that most of the model-simulated precipitation time series show poor correlation with observations. The simulation of summer precipitation in the NEC region also shows poor simulation performance, and the CMIP6 model and observation time correlation coefficients are given in Table 1. Except for the correlation coefficient between GFDL-CM4 and observations, which reaches 0.40, the correlation coefficients of the other models are less than 0.30 and do not pass the significance test. Therefore, the correlation coefficients cannot be used to measure the performance of the model in simulating the interannual variability of precipitation.

Although summer precipitation in the NEC region does not show a significant linear trend, it exhibits a non-negligible interannual variability. The IVS is a metrics for measuring model performance regarding interannual variability. The IVS takes into account the magnitude and spatial distribution of the interannual variability and scores the simulation performance of the model in simulating the interannual variability of precipitation, and the IVS closest to zero indicates that the model simulation is the best. Figure.4 shows that the CESM2 and EC-Earth3-Veg models are the worst and best models for simulating interannual precipitation variability, respectively. The IVS of most of the models are less than 0.50, which indicates that the CMIP6 model can effectively simulate the interannual variability of summer precipitation.

Figure 5 shows the ranking of the simulation performance of the 20 CMIP6 models based on different metrics. The above assessment shows that different modes show different simulation performance on different metrics, e.g., CanESM5 is ranked 3rd based on SDR, but ranked lower on SCC and RMSE. Therefore, it is necessary to combine multiple metrics to assess the simulation performance of the model (Du et al., 2022; Yang et al., 2021; Xin et al., 2020; Zhu et al., 2020).

The model's simulation performance was scored comprehensively based on SCC, SDR, RMSE, and IVS, which indicated that the closer the CRI score is to 1, the better comprehensive performance the model exhibits. The overall ranking shows that EC-Earth3-Veg has the best simulation performance and MIROC6 has the worst overall simulation performance.

The CMIP6 model simulates summer precipitation in the NEC region with significant inter-model bias (Figure.3a). The simulation of a single optimal model is not necessarily better than that of multiple models, and the uncertainty of model projection may be large if only one model is used for future projection. Therefore, based on the comprehensive ranking of each scoring index, 20 CMIP6 models were

sequentially added to the model ensemble members, and the effects of different numbers of model ensemble members on the model simulation performance were analyzed. Figure.6 shows that the simulation performance of the multi-model ensemble, except for interannual variability, increases and then decreases or remains essentially stable as the number of model ensemble members increases. The metrics SCC, RESM, and SDR show that the performance of the model simulation reaches a peak when the number of model ensemble members is selected as three. While IVS increases with the number of models, this may be due to the fact that multi-model ensemble averaging makes the simulation errors of different models cancel each other out, resulting in a small interannual variability of model-simulated precipitation. A comprehensive ranking of the simulation performance for selecting different numbers of models reveals that the ensemble consisting of the top three selected models has the best comprehensive performance. Therefore, in the subsequent precipitation assessment and projection, the models with the top three overall rankings (EC-Earth3-Veg, EC-Earth3, and MPI-ESM1-2-LR) were selected as the optimal model ensemble (HMME) in this study.

In order to validate the performance of HMME, the simulation results of HMME and Multi-Model Ensemble (MME) including 20 models were further comparatively analyzed. Figures.7a and 7c show that the spatial distribution of the precipitation simulated by HMME is closer to the observation, and the correlation coefficient between HMME and observation is 0.93, which is higher than that of MME and the single model. For the precipitation assessment in the NEC region, unlike the model ensemble selected by Yang et al. (2021), which showed no significant improvement, the HMME selected by us can effectively reduce the regional-average precipitation bias (Figure.7e). In MME, the wet bias is 14.9%, which is reduced to 8.69% in HMME. The reduction of simulation bias may mainly come from the reduction of wet bias on the southeast side of Da Xing-AN Ling Mountains.

Finally, we further compare the simulation performance of the ensemble model MME and HMME for the circulation. Figure.8 illustrates the bias of the climatological distributions of the summer sea level pressure, 850-hPa wind, 500-hPa potential height and 200-hPa latitudinal winds simulated by the MME and HMME models, as well as their bias with respect to ERA5 data. Both MME and HMME can simulate the basic characteristics of the East Asian summer monsoon. The southwesterly wind originating from the Bay of Bengal, the South China Sea and the west side of the tropical western Pacific subtropical high is the main source of water vapor for summer precipitation in the NEC region. In the western Pacific, the horizontal winds simulated by the MME and HMME show cyclonic anomalies in the south and anticyclonic anomalies in the north (Figure.8c and Figure.8e). The location of the western Pacific subtropical high at 500hPa shows a negative deviation (Figure.8d and Figure.8f), indicating that the simulated position of the western Pacific subtropical high is northerly. The biases in the MME and HMME simulations may be related to the westerly jet in the upper troposphere, because the north-south drift of the jet position is closely related to summer precipitation in the NEC region (Sun et al., 2017). The position of the westerly jet simulated by MME is northerly, and the improvement of the simulated wet bias by HMME may be due to the fact that the simulated position of the westerly jet is closer to the observation.

Figure 9 shows that there is no significant change trend in summer precipitation in NEC from 1979 to 2014. Both MME and HMME can simulate this characteristic of precipitation in historical periods. Compared with MME, HMME narrows the uncertainty interval of precipitation. The average daily precipitation simulated by HMME varies from 1.87 to 5.87mm/day, which is closer to the observation of 2.85-4.94mm/day. This shows that HMME effectively reduces the uncertainty of summer precipitation in NEC. Although the correlation coefficient between the observed and HMME simulated precipitation time series is -0.16, there is no improvement compared with the MME-observed ones. However, HMME improves the simulation of interannual variability by reducing the number of models in the ensemble. The ratio of standard deviations between HMME and observations is 0.68, indicating that HMME is closer to observations.

In general, the main Bias of the CMIP6 model in simulating summer precipitation in the NEC is due to the overestimation of precipitation in the southeastern part of the Greater Khingan Range. The HMME simulation bias in this region still exists, but the magnitude is reduced. Furthermore, HMME exhibits higher skill in reproducing the interannual variability of precipitation.

4. Future Projection

Figure.10 shows the time series of regionally averaged summer precipitation anomaly changes in NEC under the HMME historical experiment and the SSP245 and SSP585 scenarios. SSP245 represents an integrated scenario of medium-emission socioeconomic development pathways with low and medium radiative forcing. SSP585 represents a combined scenario of a high-emission future socio-economic development pathway and strong radiative forcing, under which global greenhouse gas emissions will continue to increase rapidly. This leads to an increase in the concentration of greenhouse gases in the atmosphere, which in turn triggers a sustained and pronounced global warming. As can be seen from Figure.10a, the overall average daily precipitation in summer will show a significant increasing trend in the future. The increase in the SSP585 scenario (0.15mm/10a) is larger than that in the SSP245 scenario (0.05mm/10a). In the near term (2021–2040), mid-term (2051–2070) and long-term (2081–2100) of the 21st century, the precipitation increments are 9.24%, 15.54% and 31.95% respectively. Figure.10(b-c) further shows the spatial distribution of long-term precipitation changes in the 21st century. In the future, summer precipitation in the NEC will increase as a whole, and the amplitude of precipitation change will generally decrease from south to north. However, precipitation trends vary in different regions at different times (Figure.11). Under the SSP245 scenario, precipitation in the eastern part of NEC shows an increasing trend in the near term and a significant decreasing trend in the mid-term in the 21st century. Under the SSP585 scenario, except for the decreasing trend in the eastern part of NEC in the mid-21st century, the entire region shows a significant increasing trend in precipitation.

5. Conclusions.

In this paper, we evaluated the performance of 20 CMIP6 models to simulate summer precipitation in NEC over the period 1979–2014, and the error metrics and interannual variability of the Taylor diagram were

comprehensively ranked. The optimal models with higher score were further selected to constitute the HMME, and the biases among different model ensembles were compared, and further projected precipitation for the years 2015–2100. The main conclusions are summarized below:

1. The model can basically reproduce the spatial distribution of the summer precipitation in NEC that decreases from southeast to northwest. However, there is a wet bias on the southeast side of the Da Xing-AN Ling. EC-Earth3 performs the best in terms of spatial distribution.
2. The modeled precipitation time series have poor correlation with observations and cannot reproduce the intra-annual changes. However, for interannual variability, most models show good simulation skills.
3. The top three EC-Earth3-Veg, EC-Earth3, and MPI-ESM1-2-LR were selected to form the HMME based on the rankings of the composite indexes. The HMME outperformed the MME in terms of the spatial distribution and interannual variability, and significantly reduced the wet bias on the southeastern side of the Da Xing-AN Ling Mountains.
4. Under the SSP245 and SSP585 scenarios, precipitation in NEC shows a consistent increasing trend, with the largest increase in the southern region where precipitation is high. The precipitation growth rate under the SSP585 scenario is faster than that under the SSP245 scenario. Under the SSP245 scenario, precipitation in the eastern region shows a decreasing trend in the mid-21st century.

Precipitation bias is affected by many factors. Zhou et al. (2023) pointed out that the northeast cold vortex simulated by the model is more northerly, and Xin et al. (2020) pointed out that CMIP6 can reasonably reproduce the anticyclonic anomalies in the western Pacific. Precipitation distribution can be reproduced and predicted more accurately using a combination of statistical and dynamic methods (Liang et al., 2019; Ding and Gao, 2021). Further analysis is needed to analyze other physical quantities simulated by the CMIP6 model and find suitable predictors.

Declarations

Conflict of interest The authors have no known competing financial interests or personal relationships . The authors have no relevant financial or non-financial interests to disclose.

Ethical approval

Ethics approval was not required for this research.

Author contributions

Material preparation, data collection, and analysis were performed by JX and LL. The first draft of the manuscript was written by JX and LL. LL performed supervision, and reviewed paper and takes charge of revision work for paper revision. All authors read and approved the final manuscript.

Funding

This work was supported by The National Natural Science Foundation of China (Grant numbers 42375002).

Data availability

The original datasets analyzed during the current study are available in the repositories [National Center for Meteorological Sciences (data.cma.cn), The Earth System Grid Federation (esgf-node.llnl.gov/projects/cmip6)].

References

1. Chen WL, Jiang ZH, Li L (2011) Probabilistic Projections of Climate Change over China under the SRES A1B Scenario Using 28 AOGCMs. J Clim 24:4741–4756
2. Ding T, Gao H (2021) A feasible approach to improve forecast skill of summer precipitation in northeast China by statistical regression of the northeast China cold vortex in the multimodel ensemble. Int J Climatol 41(14):6397–6414
3. Donat MG, Delgado-Torres C, De Luca P, Mahmood R, Ortega P, P., and, Doblas-Reyes FJ (2023) : How credibly do CMIP6 simulations capture historical mean and extreme precipitation changes? Geo Res Lett, 50, e2022GL102466.
4. Dong TY, Dong WJ (2021) Evaluation of extreme precipitation over Asia in CMIP6 models. Clim Dyn 57:1751–1769
5. Du Y, Wang DG, Zhu JX, Wang DY, Qi XX, Cai JH (2022) Comprehensive assessment of CMIP5 and CMIP6 models in simulating and projecting precipitation over the global land. Int J Climatol 42(13):6859–6875
6. Eyring V, Bony S, Meehl GA, Senior CA, Stevens B, Stouffer RJ, Taylor KE (2016) Overview of the Coupled Model Intercomparison Project Phase 6 (CMIP6) experimental design and organization. Geosci Model Dev 9:1937–1958
7. Gao J, Gao H (2018) Influence of the northeast cold vortex on flooding in northeast China in summer 2013. J Meteorol Res 32(2):172–180
8. Gao Z, Hu ZZ, Zhu JH, Yang S, Zhang RH, Xiao ZN, Jha B (2014b) Variability of summer rainfall in Northeast China and its connection with spring rainfall variability in the Huang-Huai region and Indian Ocean SST. J Clim 27:7086–7101
9. Gao Z, Hu ZZ, Jha B, Yang S, Zhu JH, Shen BZ, Zhang RJ (2014a) Variability and predictability of Northeast China climate during 1948–2012. Clim Dyn 43:787–804
10. Han TT, Zhang MH, Zhu JW, Zhou BT, Li SF (2021) Impact of early spring sea ice in Barents Sea on midsummer rainfall distribution at Northeast China. Clim Dyn 57:1023–1037
11. Han TT, He SP, Wang HJ, Hao X (2018) Enhanced influence of early-spring tropical Indian Ocean SST on the following early-summer precipitation over Northeast China. Clim Dyn 51:4065–4076

12. He BH, Sun JQ, Yu ET, Wang HJ, Zhang MQ, Hua W (2020) Simulation Study on the Influence of the Great Khingan Strip and Changbai Mountain on Summer Rainfall in Northeast China. Clim Environ Res 25(3):268–280 (in Chinese with English abstract)
13. He LQ, Zhou TJ, Chen XL (2023) South Asian summer rainfall from CMIP3 to CMIP6 models: biases and improvements. Clim Dyn 61:1049–1061
14. Intergovernmental Panel on Climate Change (IPCC) (2023) : *Climate Change 2023: Summary for Policymakers*, in the Sixth Assessment Report of the Intergovernmental Panel on Climate Change, Core Writing Team, H. Lee and J. Romero (eds.), Geneva, Switzerland, pp. 1–34
15. Jia QM, Jia HF, Li YJ, Yin DK (2023) Applicability of CMIP5 and CMIP6 Models in China: Reproducibility of Historical Simulation and Uncertainty of Future Projection. J Clim 36:5809–5824
16. Jiang DB, Hu D, Tian ZP, Lang XM (2020) Differences between CMIP6 and CMIP5 models in simulating climate over China and the East Asian monsoon. Adv Atmos Sci 37(10):1102–1118
17. Jiang ZH, Li W, Xu JJ, Li L (2015) Extreme precipitation indices over China in CMIP5 models. Part I: Model evaluation. J Clim 28:8603–8619
18. Liang LQ, Li LJ, Liu Q (2011) Precipitation variability in Northeast China from 1961 to 2008. J Hydrol 404(1):67–76
19. Liang P, Hu ZZ, Liu YY, Yuan X, Li XF, Jiang XW (2019) Challenges in predicting and simulating summer rainfall in the eastern China. Clim Dyn 52:2217–2233
20. Liu S, Coauthors (2010) Time–Frequency Characteristics of Regional Climate over Northeast China and Their Relationships with Atmospheric Circulation Patterns. J Clim 23:4956–4972
21. Mao Y, Wu GC, Xu GZ, Wang KC (2022) Reduction in Precipitation Seasonality in China from 1960 to 2018. J Clim 35(1):227–248
22. Pierce DW, Barnett TP, Santer BD, Gleckler PJ (2009) : Selecting global climate models for regional climate change studies. *Proc. Natl. Acad. Sci. U.S.A.*, 106, 8441–8446
23. Shen BZ, Lin ZD, Lu RY, Yian Y (2011) Circulation Anomalies Associated with Interannual Variation of Early- and Late-Summer Precipitation in Northeast China. Sci China Earth Sci 54(7):1095–1104
24. Stouffer RJ, Eyring V, Meehl GA, Bony S, Senior C, Stevens B, Taylor KE (2017) CMIP5 scientific gaps and recommendations for CMIP6. Bull Am Meteorol Soc 98:95–105
25. Sun L, Shen BZ, Sui B, Huang BH (2017) The influences of East Asian Monsoon on summer precipitation in Northeast China. Clim Dyn 48:1647–1659
26. Tao CW, Jiang C, Sun JX (2016) Projection of future changes in climate in Northeast China using a CMIP5 multi-model ensemble. Chin J Phys 59(10):3580–3591 (in Chinese with English abstract)
27. Taylor KE (2001) Summarizing multiple aspects of model performance in a single diagram. J Geophys Res 106:7183–7192
28. Wu J, Gao XJ (2013) A gridded daily observation dataset over China region and comparison with the other datasets. Chin J Phys 56(4):1102–1111 (in Chinese with English abstract)

29. Wu RG, Yang S, Liu S, Sun L, Lian Y, Gao Z (2011) Northeast China summer temperature and North Atlantic SST. J Geophys Res 116:D16116
30. Xin XG, Wu TW, Zhang J, Yao JC, Fang YJ (2020) Comparison of CMIP6 and CMIP5 simulations of precipitation in China and the East Asian summer monsoon. Int J Climatol 40:6423–6440
31. Xu LL, Zhang TT, Yu W, Yang S (2023) Changes in concurrent precipitation and temperature extremes over the Asian monsoon region: observation and projection. Environ Res Lett 18(4):044021
32. Xu Y, Gao XJ, Shen Y, Xu CH, Shi Y, Giorgi F (2009) A daily temperature dataset over China and its application in validating a RCM simulation. Adv Atmos Sci 26:763–772
33. Yang XL, Zhou BT, Xu Y, Han ZY (2021) CMIP6 evaluation and projection of temperature and precipitation over China. Adv Atmos Sci 38(5):817–830
34. Yao XP, Dong M (2000) Research on the features of summer rainfall in Northeast China. Quarterly. J Appl Meteor 11:297–303 (in Chinese with English abstract)
35. Zhao JH, Zhou J, Yang L, Wei H, Feng GL (2018) Inter-annual and inter-decadal variability of early- and late-summer precipitation over Northeast China and their background circulation. Int J Climatol 38(6):2880–2888
36. Zhou TJ, Zou LW, Chen XL (2019) : Commentary on the Coupled Model Intercomparison Project Phase 6 (CMIP6). *Climate Change Research*, 15, 445 – 456. (in Chinese with English abstract)
37. Zhou TJ, Xie ZW, Bueh C, Chen LQ, Li SF, Yang X (2023) : Evaluation of spatial–temporal features and circulation patterns of Northeast China cold vortex in CMIP6 AMIP simulations. *Clim. Dyn.*, publish online, 10.1007/s00382-023-06875-8
38. Zhu HH, Jiang ZH, Li J, Li W, Sun CX, Li L (2020) Does CMIP6 Inspire More Confidence in Simulating Climate Extremes over China? Adv Atmos Sci 37:1119–1132

Figures

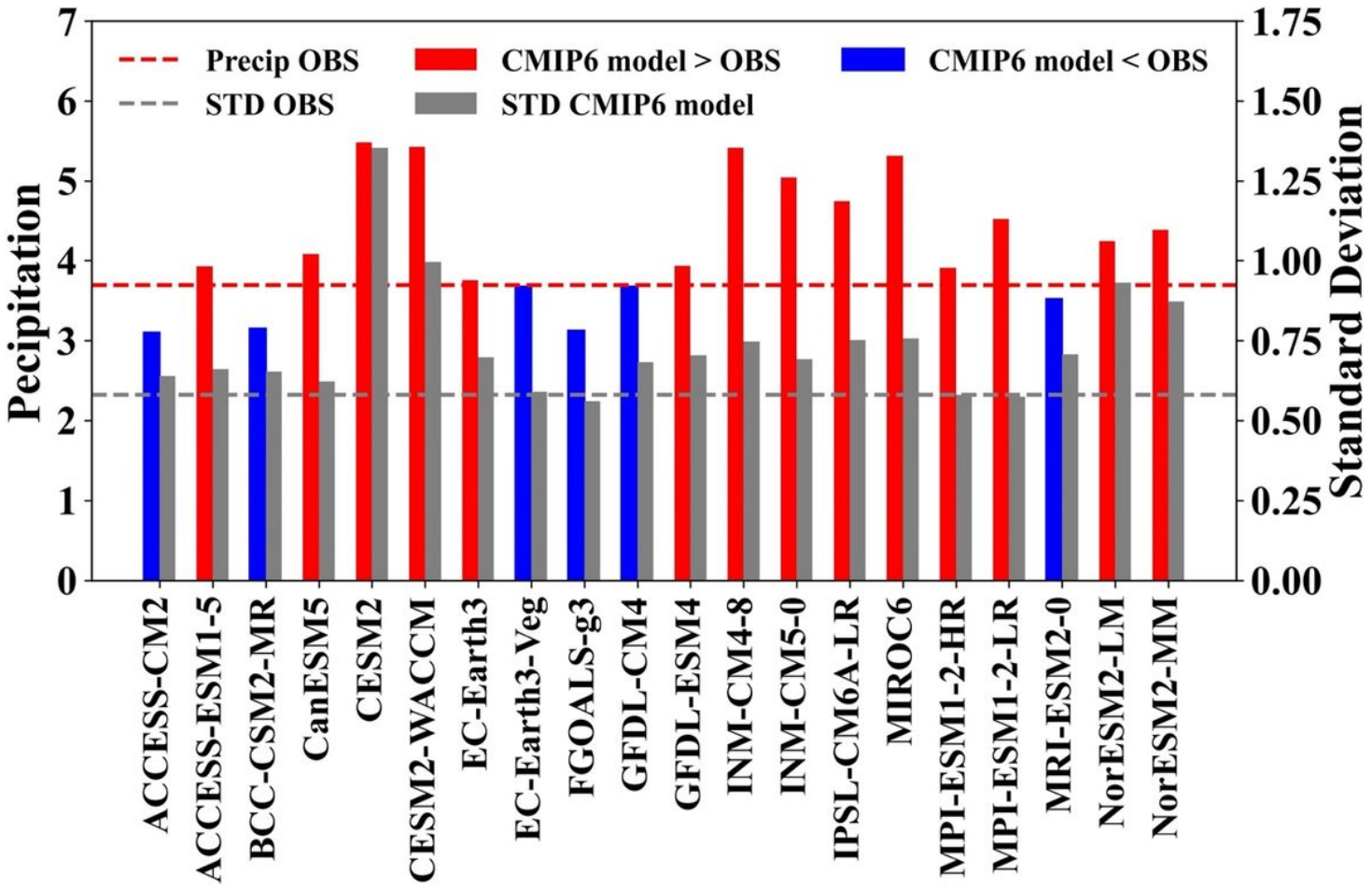

Figure 1

The regional summer mean daily precipitation (Blue bars indicate an underestimation of the pattern and red bars indicate an overestimation of the pattern, with values corresponding to the left-hand axis.) and standard deviation (Gray, corresponding to the right axis) in the NEC, 1979-2014, as simulated by the CMIP6 model history experiment. The red dashed line in the figure shows the observed mean precipitation and the gray dashed line shows the observed standard deviation (Unit: mm/day).

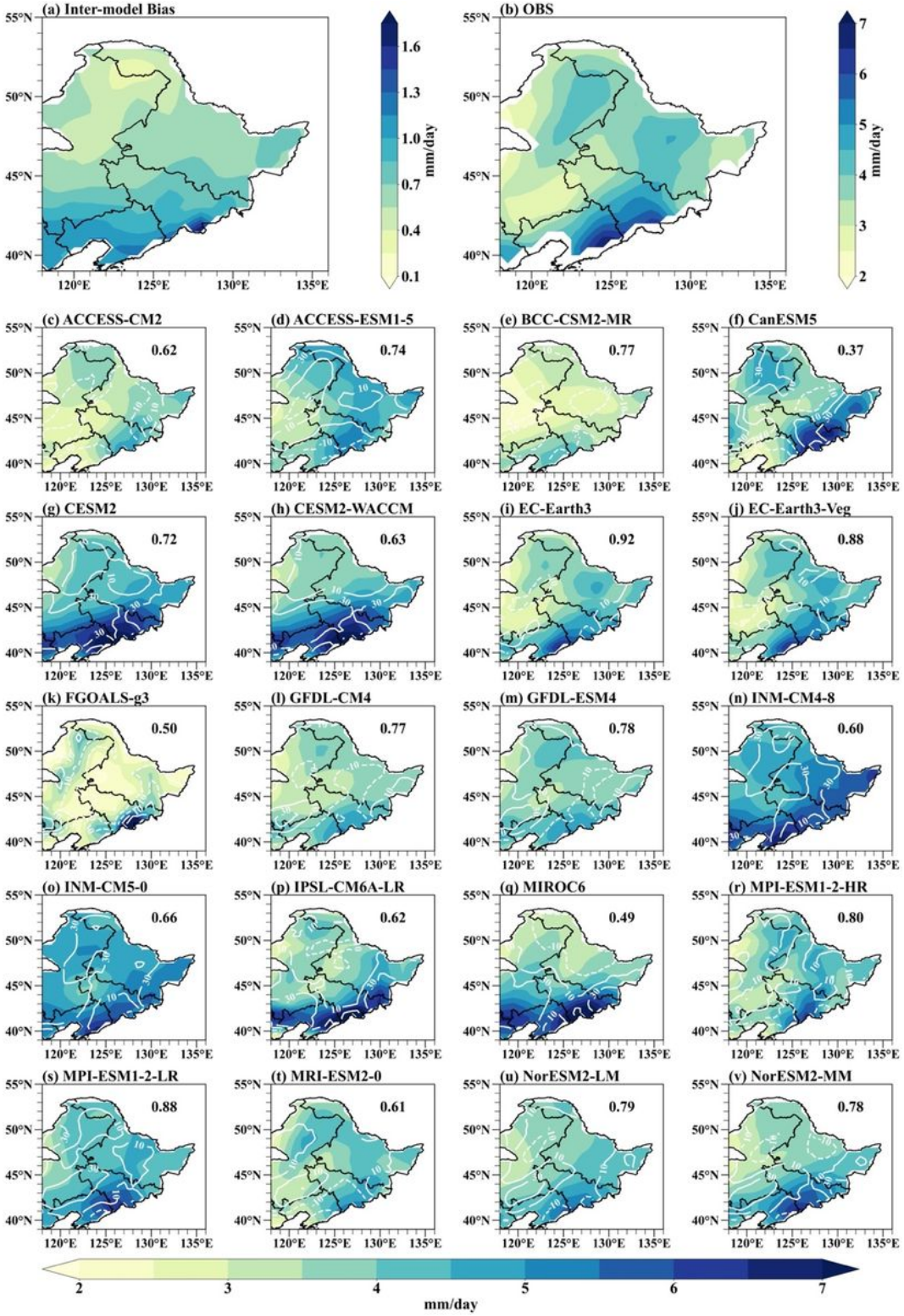

Figure 2

Pattern of inter-model bias (a), observed and CMIP6 modeled (b-v) mean daily precipitation (colors: mm/day) in NEC region, 1979-2014. The white contours are the relative bias between simulated and observed precipitation, and the black numbers labeled in the figure are the spatial correlation coefficients between simulated and observed precipitation.

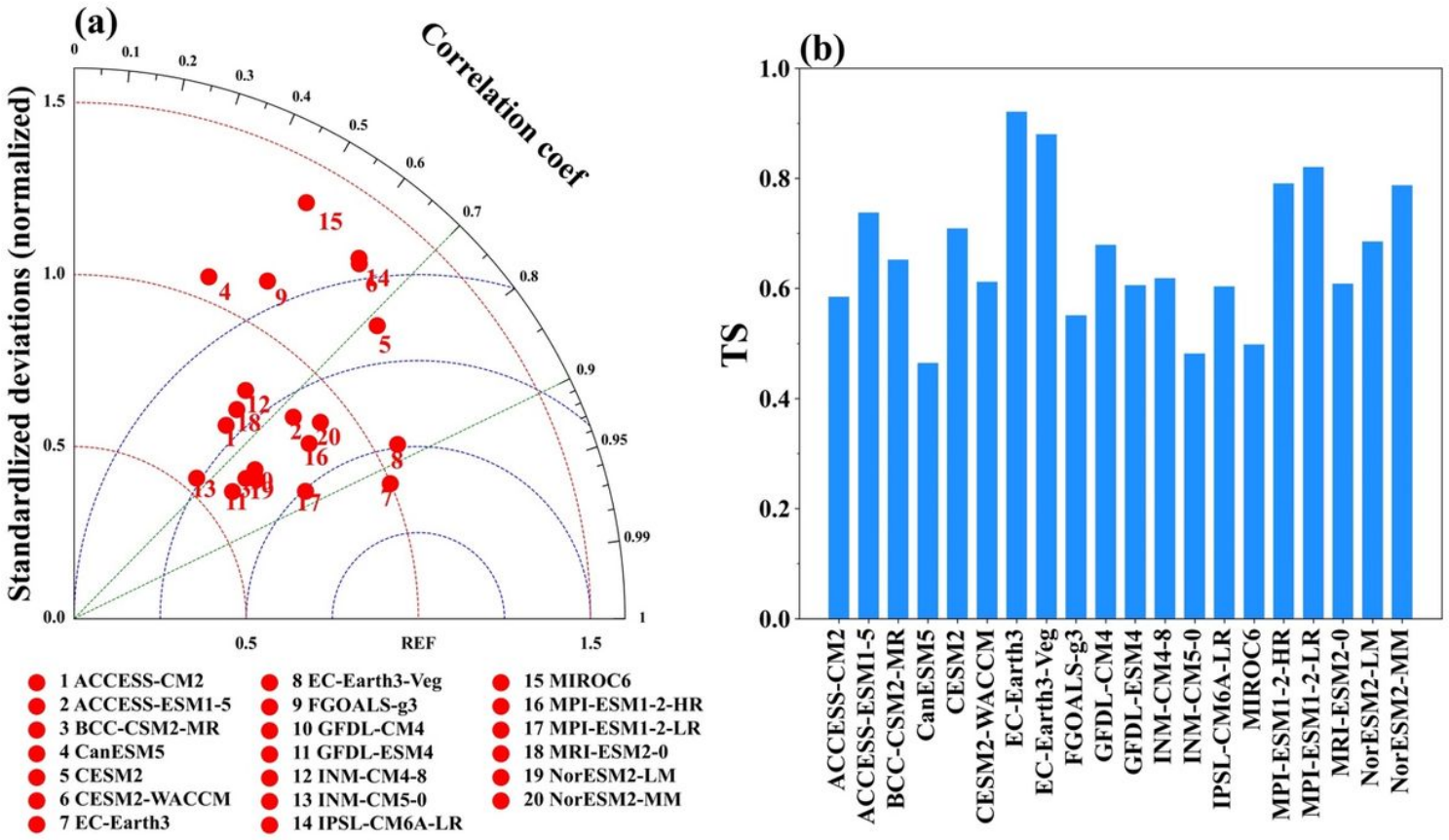

Figure 3

(a) Taylor diagram of summer precipitation (Unit: mm/day) in the NEC during 1979 - 2014 and (b) scores (TS) for each model.

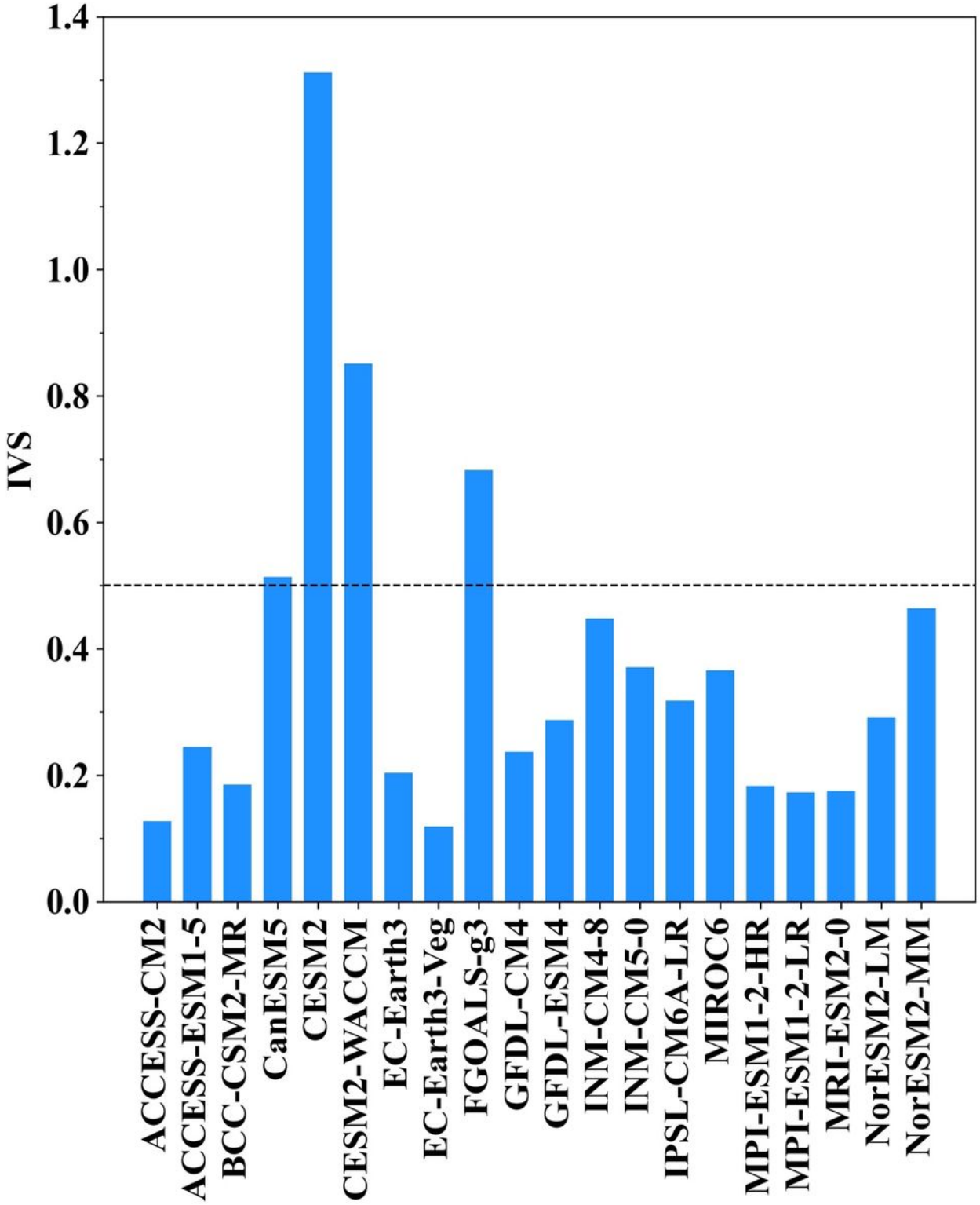

Figure 4

Skill score (IVS) for interannual variability of summer precipitation in the NEC region during 1979 - 2014.

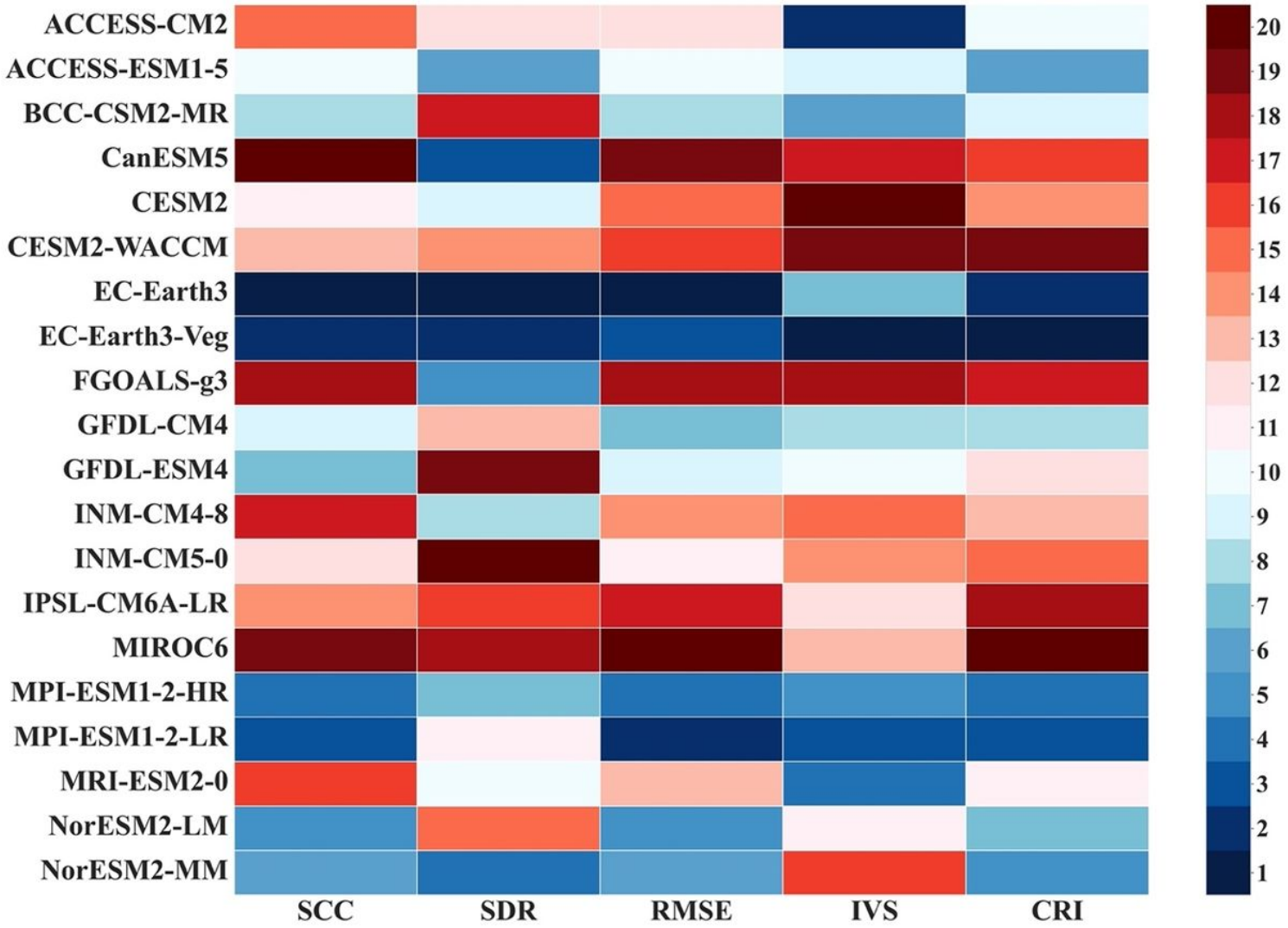

Figure 5

Based on 20 CMIP6 modes, ranked according to SCC, SDR, RMSE, IVS, and CRI, with smaller numbers indicating better performance in model simulation.

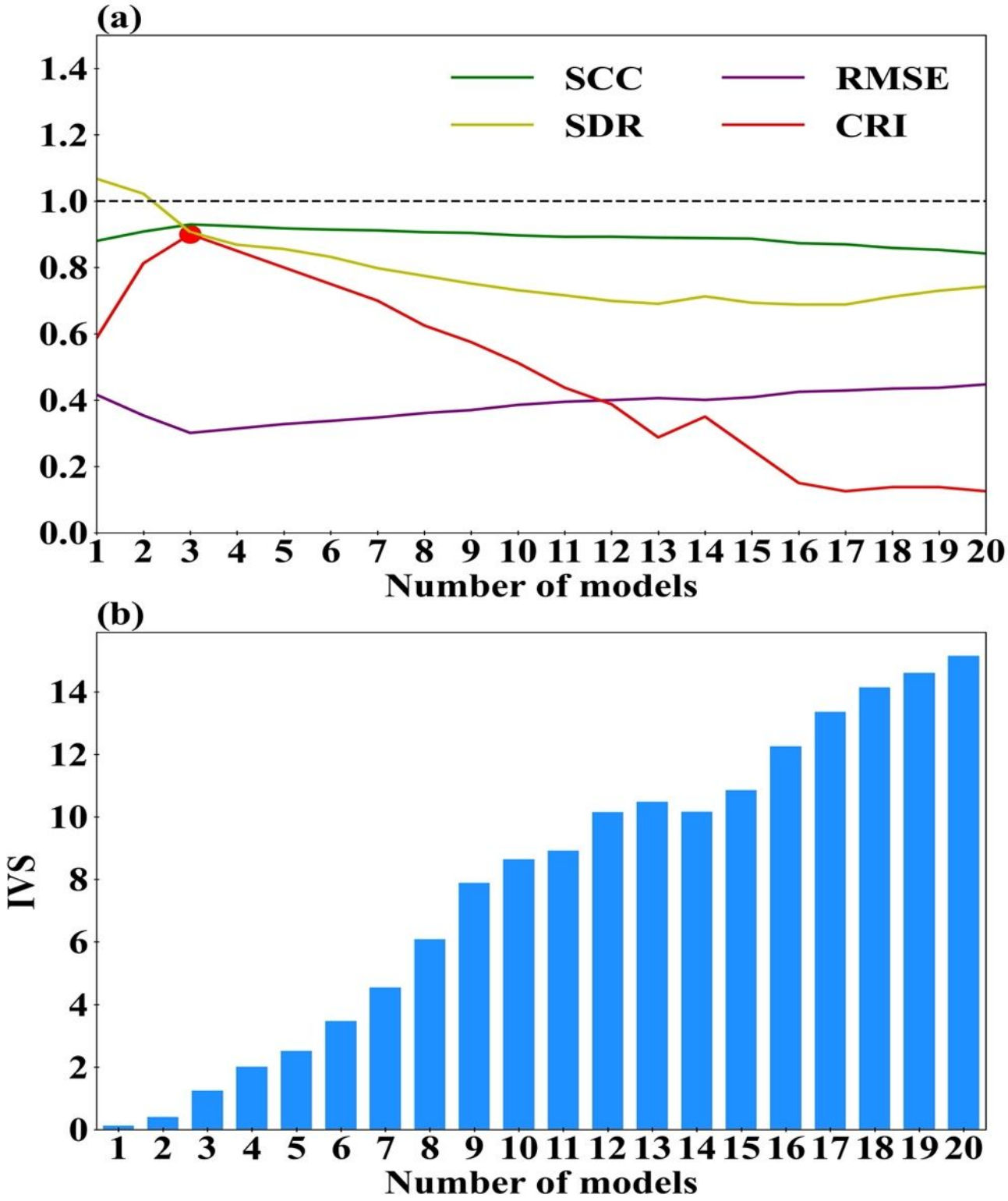

Figure 6

(a) Variation of SCC (green), SDR (yellow), RMSE (purple) and (b) IVS vary with the number of multi-model ensemble members, and CRI (red) reflects the composite ranking.

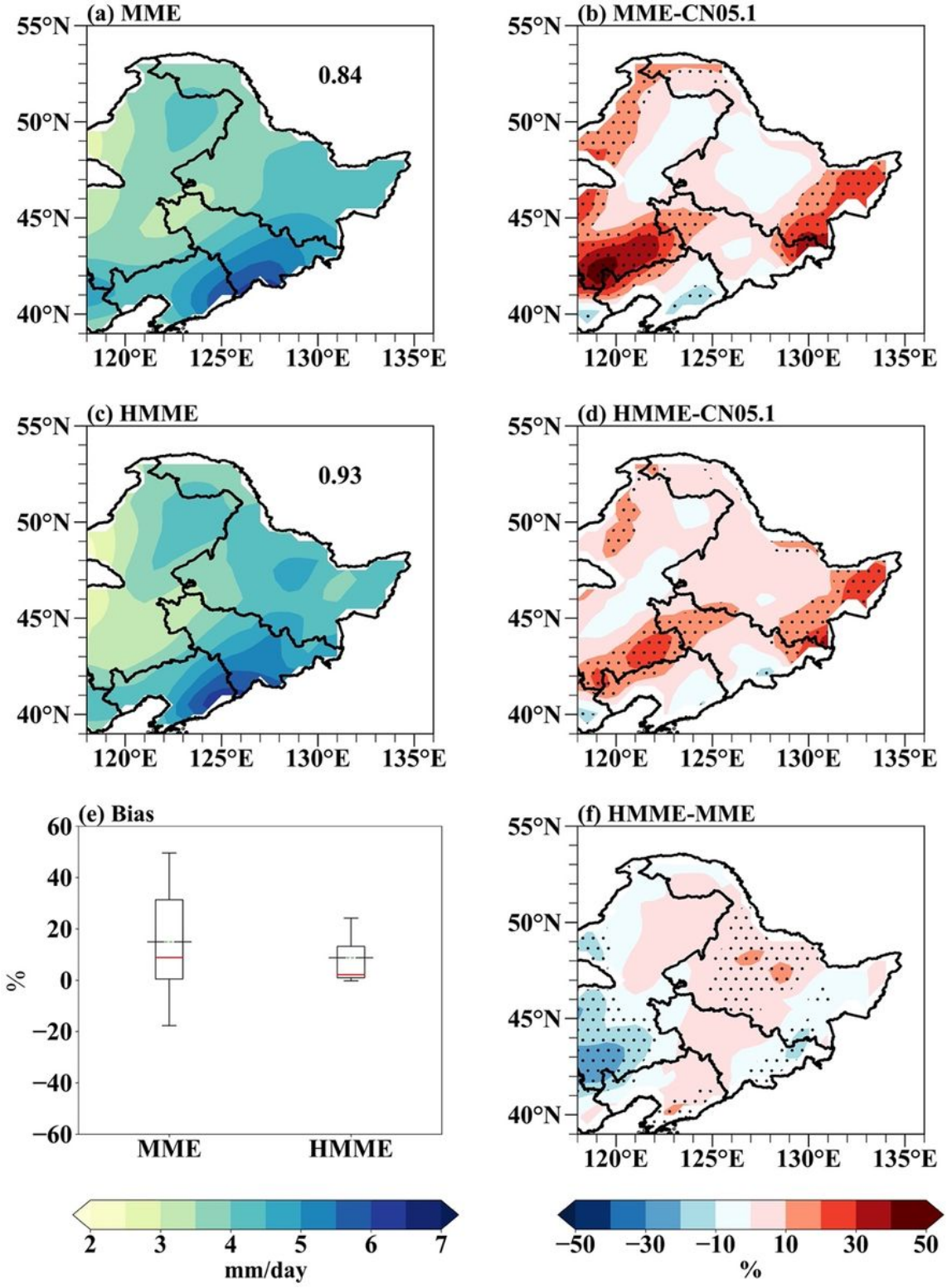

Figure 7

Modeled precipitation and its bias by MME (a-b) and HMME (c-d) with the labeled numbers being the SCC. (e) represents the regional-average precipitation bias, with the long black line being the multi-model mean and the red line being the median, and (f) denotes the difference between HMME and MME.

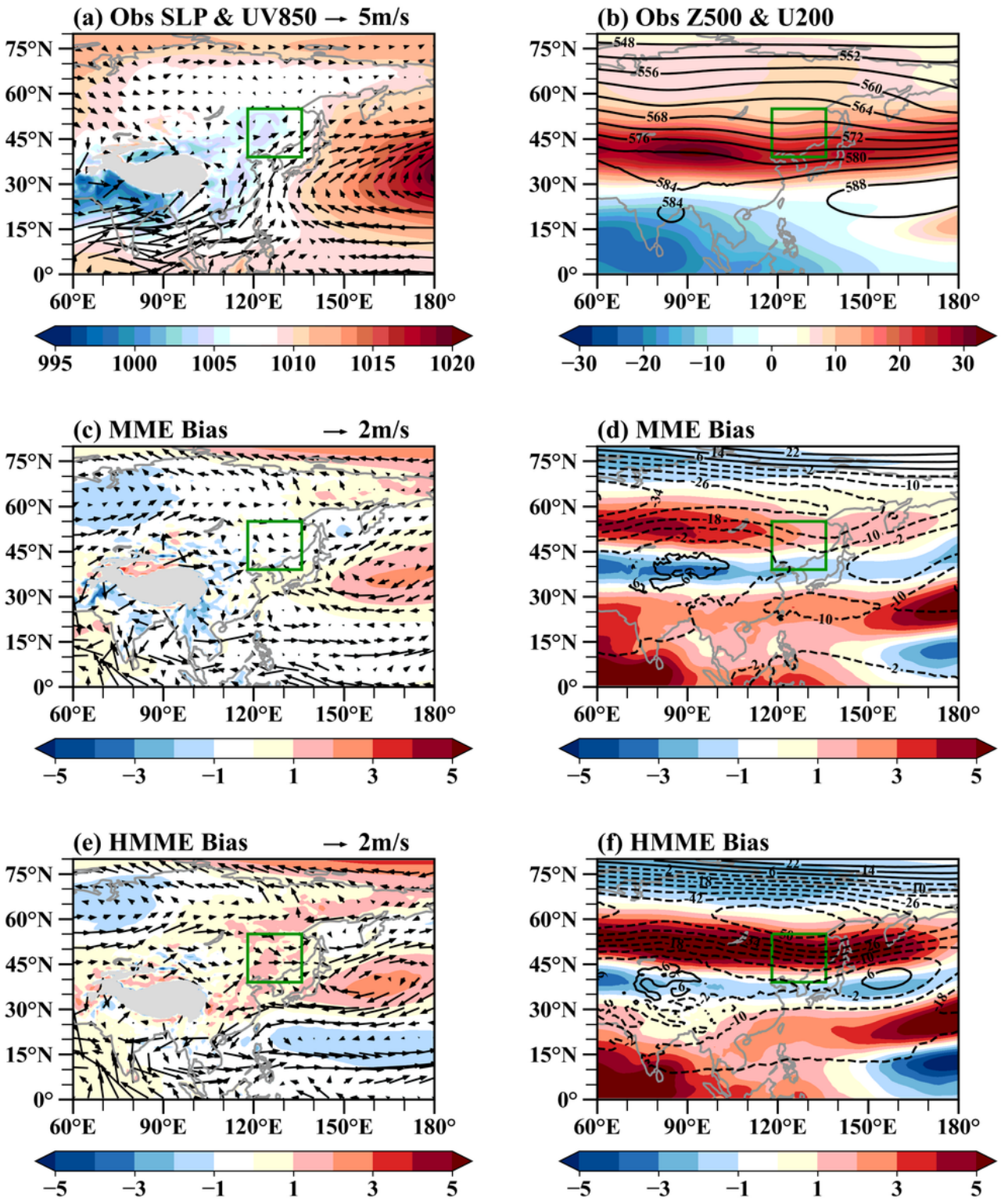

Figure 8

Climatological distribution of summer sea-level pressure, 850-hPa wind, 500-hPa potential height, and 200-hPa latitudinal winds for ERA5 data during 1979-2014 (a-b), and the modeled bias of MME (c-d) and HMME (e-f).

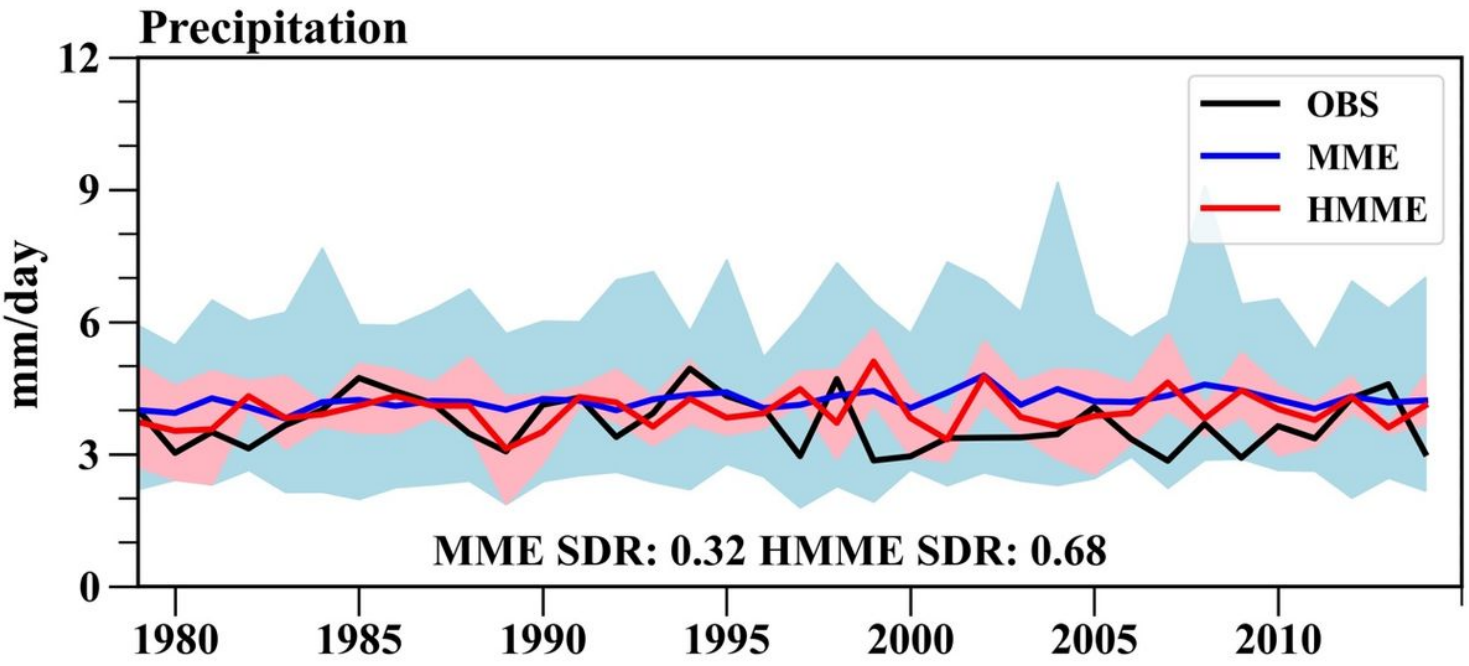

Figure 9

The modeled regional average precipitation during the historical period, and with shading indicating the model-simulated precipitation amplitude within the ensemble.

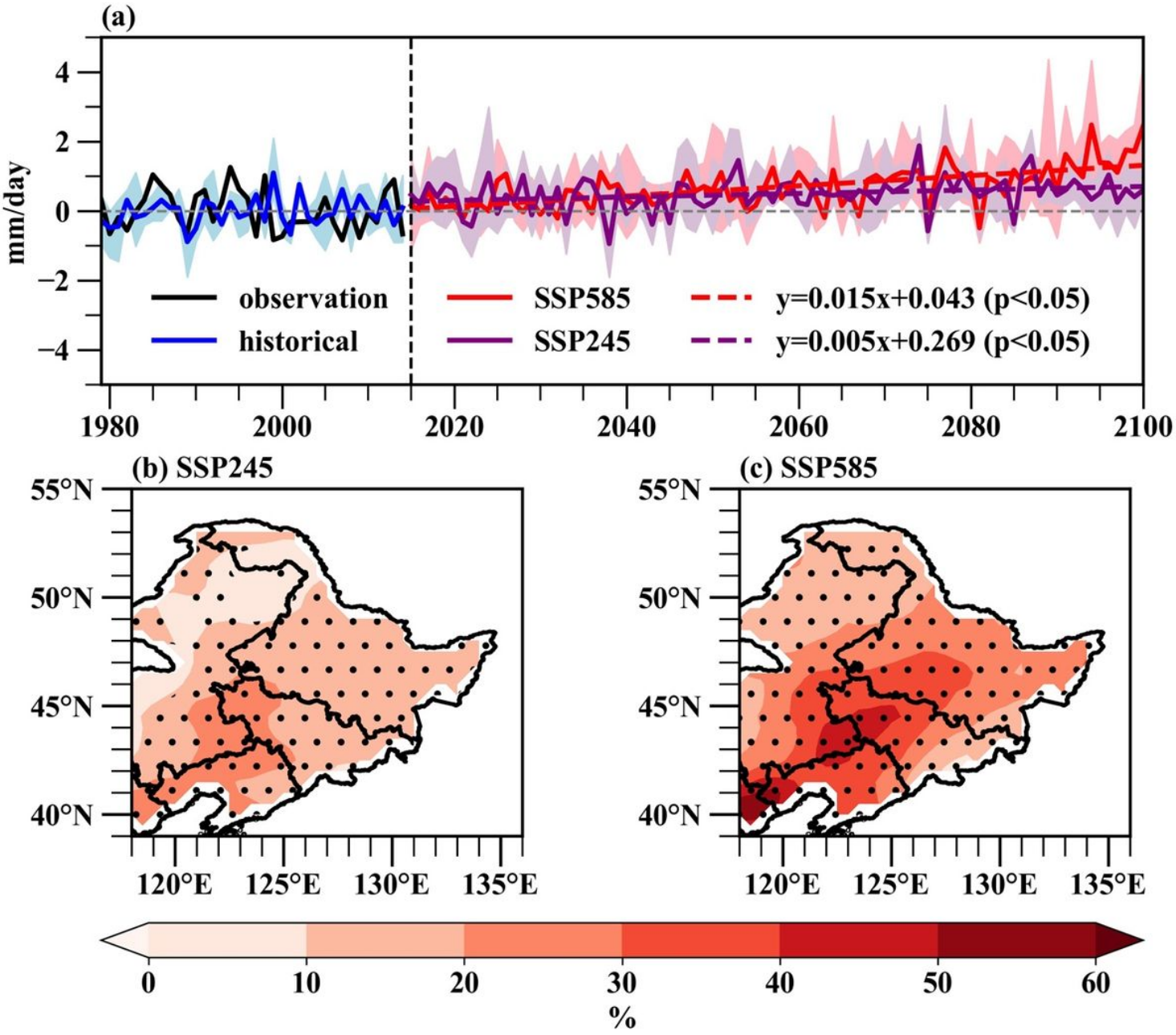

Figure 10

Time series of observed (black), HMME historical simulations (blue), and projected regional-averaged summer daily precipitation in NEC under the SSP245 (purple) and SSP585 (red) scenarios. The red dashed line shows the projected future trend. (b) and (c) are trends in precipitation relative to the climate base period for 2081-2100 under the SSP245 and SSP585 scenarios, respectively.

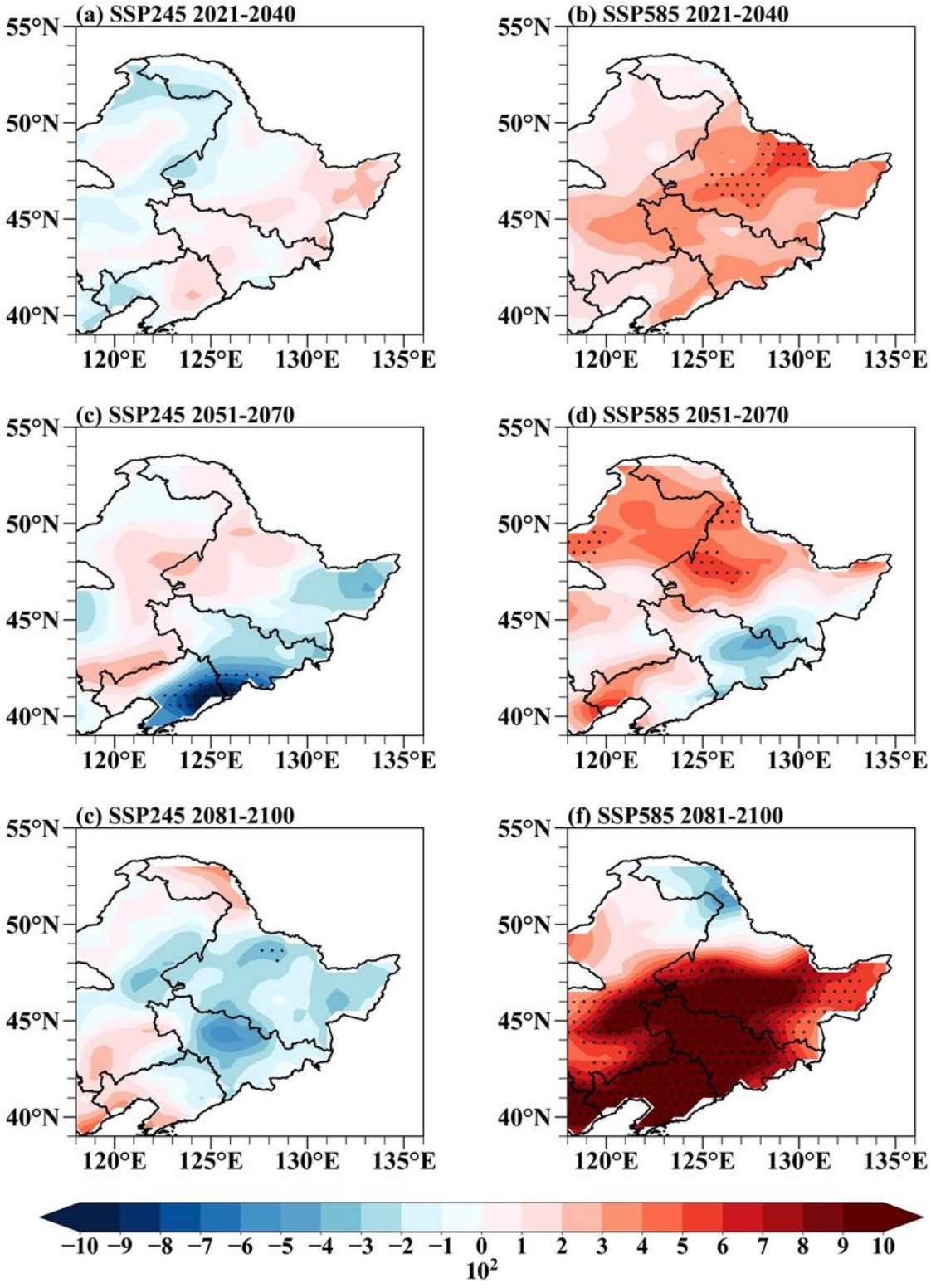

Figure 11

Precipitation change under SSP245 and SSP585 scenarios in the near term (2021-2040), mid-term (2051-2070) and long-term (2081-2100) of the 21st century.